



Macro- and microphysical characteristics of snowfall and non-snowfall clouds in the West Tianshan Mountains of China based on cloud radar

Jinru Zhang^{1,2,3} · Haoran Li⁴ · Yong Zeng^{1,2,3} · Lianmei Yang^{1,2,3} · Jiangan Li^{1,2,3}

Received: 30 April 2021 / Accepted: 4 July 2022
© The Author(s) 2022, corrected publication 2023

Abstract

The macro- and microphysical characteristics of wintertime precipitating clouds and non-precipitating clouds over the West Tianshan Mountains, China, were analyzed with the use of Ka-band radar and weighing rain gauge observations. The data were collected from January to February 2019, December 2019, and from December 2020 to February 2021. Snowfall clouds mainly ranged from 0.15~2.50 km and had a reflectivity (Z) of mostly 10~33 dBZ. Non-snowfall clouds were primarily distributed within the height range of 2~8 km, and the Z values were within the range of -22~15 dBZ. Compared with non-snowfall clouds, snowfall clouds have a higher particle water content (M) but a similar radial velocity (V). Light and moderate snowfall clouds were mainly located at heights of 0.15~3.50 km and had Z values concentrated from 5~24 dBZ. Heavy snowfall clouds were characterized by a Z of 5~30 dBZ below 3.5 km. The proportion of clouds with an M value $> 0.1 \text{ g}\cdot\text{m}^{-3}$ below 2 km was noticeably higher for heavy snow events than for light and moderate snow events. The differences in the distributions and values of snowfall cloud V values were small among the different snow types, and descending motions occurred below 6 km, with V ranging -1.4~-0.3 $\text{m}\cdot\text{s}^{-1}$. The heights of the non-snowfall cloud top and base during the day were lower than those at night. The snowfall cloud top did not show noticeable diurnal variations. The cloud top and base heights of the non-snowfall clouds both showed a single-peak distribution. The cloud top values of snowfall clouds exhibited bimodal distributions.

Responsible Editor: Sang-Woo Kim.

✉ Lianmei Yang
yanglm@idm.cn

✉ Jiangan Li
shzljg_qxj@163.com; 1139464699@qq.com

Jinru Zhang
751639350@qq.com

Haoran Li
haoran.li@helsinki.fi

Yong Zeng
zengyong@idm.cn

- ¹ Institute of Desert Meteorology, China Meteorological Administration, Urumqi 830002, China
- ² Xinjiang Cloud Precipitation Physics and Cloud Water Resources Development Laboratory, Urumqi 830002, China
- ³ Field Scientific Observation Base of Cloud Precipitation Physics in West Tianshan Mountains, Urumqi 830002, China
- ⁴ Institute for Atmospheric and Earth System Research / Physics, Faculty of Science, University of Helsinki, Helsinki, Finland

1 Introduction

Clouds, as one of the primary factors influencing weather and climate changes, influence the energy balance and water circulation of the Earth by altering the radiative forcings and atmospheric thermal motions (Clement et al. 2009; Zhou et al. 2016). The cloud radiation effect is primarily determined by the macro- and microphysical properties of the cloud. Therefore, the observations, inversions, and research on the macroscopic and microscopic physical properties of clouds are important for improving the parameterization processing of clouds in Models and understanding the feedback effect of clouds in climate change (Ackerman and Stokes, 2003; Harrison et al. 1990). At present, the macro- and microphysical characteristics of clouds are mainly observed and studied by aircraft, satellites, and ground-based equipment (Chen et al. 2016; Li et al. 2017; Reddy et al. 2018; Yin et al. 2013). Although aircraft can obtain detailed observation results, the sampling space is small, and the cost is high (Parish and Leon, 2013). Satellites have a wide detection range but low spatial and temporal resolutions (Yi, 2019).

Millimeter-wave cloud radar has high sensitivity and spatial–temporal resolution (Zeng et al. 2020a), and it can continuously observe clouds and obtain the macro- and micro-physical vertical structure characteristics of clouds through reflectivity, radial velocity, and other products. Therefore, millimeter-wave cloud radar is a powerful tool for studying the macro- and microproperties of clouds. (Kollias et al. 2011; Zeng et al. 2020b). In China, researchers have conducted research only in central and eastern China and the Qinghai–Tibet Plateau (Zhao et al. 2016; Li et al. 2017). Zhang et al. (2019b) observed the vertical structure of clouds in Beijing based on cloud radar data and found that the cloud top height and radar reflectivity in summer and autumn were higher than those in spring and winter and that there were two peak values in the height of the cloud base (0~1 km and 5~6 km). Wang et al. (2017) used cloud radar to analyze the microphysical and dynamic characteristics of freezing rain and snowfall in Weining, Guizhou, and the results showed that the average radii of the particles at the beginning of freezing rain and snowfall were approximately 40 μm and 120 μm , respectively. Qiu et al. (2018) used cloud radar to analyze the vertical structure and water content of clouds over the Qinghai–Tibet Plateau in summer and found that at local times of 00:00–06:00, 06:00–12:00, 12:00–18:00, and 18:00–24:00, the occurrence probabilities of clouds were 82.7%, 56.2%, 55.3%, and 65.4%, respectively. This type of research is of great significance for understanding

the physical characteristics of clouds and precipitation in China. However, there are still few studies on the snowfall process in arid areas of China using millimeter-wave cloud radar (Zeng et al. 2020a).

The Xinjiang Uyghur Autonomous Region has an arid and semiarid climate. However, because of the special topography involving three mountain ranges separated by two basins, Xinjiang, particularly northern Xinjiang, where polar front jets frequently move southwards in winter, is the region with the most frequent snowfall and one of the three regions with the most snow cover in China in winter (Li 1998). Although a number of scholars have investigated the structural characteristics of non-precipitating clouds and precipitating clouds in China based on satellite observation data (Luo et al. 2011; Qie et al. 2014; Xu 2013), research on the physical characteristics of non-snowfall clouds and snowfall clouds in Xinjiang in winter has rarely been reported. The West Tianshan Mountains are the precipitation center of Xinjiang (Zhang and Yang 2018), and Xinyuan is one of the best representative areas in terms of precipitation in the West Tianshan Mountains. On January 22, 2019, a millimeter-wave cloud radar was installed at the Xinyuan weather station (43°27'N, 83°18'E; altitude: 928 m) (Fig. 1) by the Institute of Desert Meteorology, CMA, Urumqi. In this study, we analyzed the structural characteristics of the non-snowfall clouds and snowfall clouds of different snowfall magnitudes at Xinyuan station from January to February

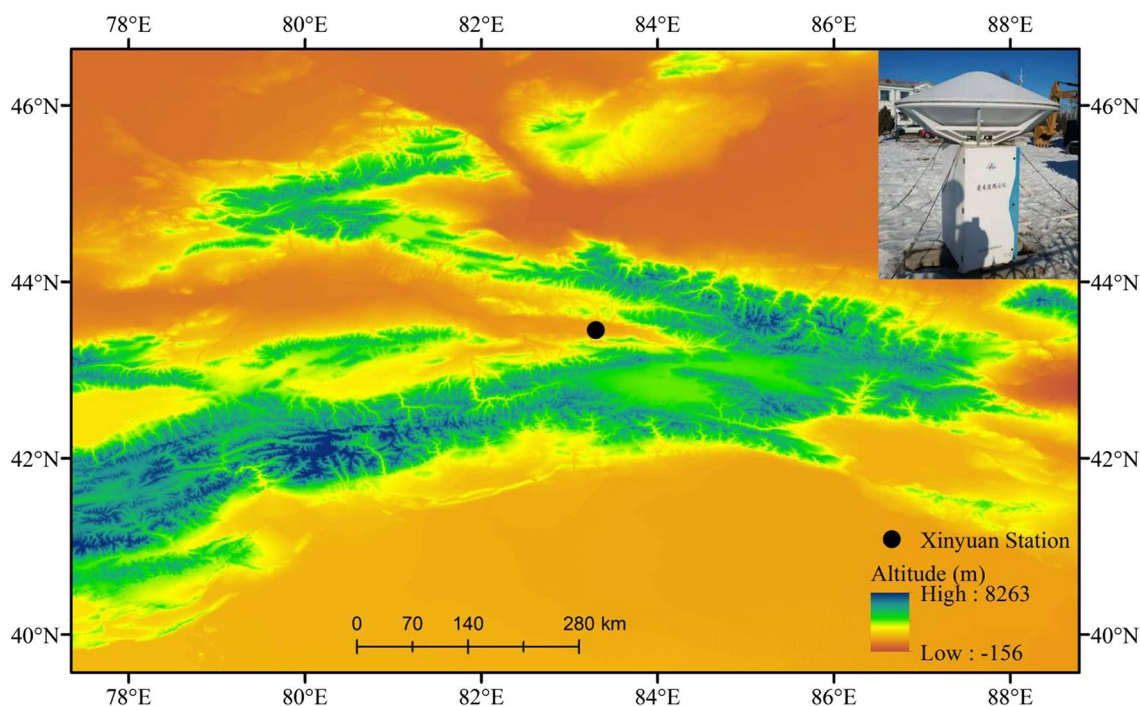


Fig. 1 Location of Xinyuan Meteorological Station (XY, 83°18' E, 43°27' N, 928 m above sea level) and photos of the millimeter-wave cloud radar instrument

2019, December 2019, and December 2020 to February 2021 (in winter). To achieve this goal, we used radar observation data on the cloud radar reflectivity, radial velocity, height of the cloud base, cloud top parameters, and moisture content of snow particles obtained through inversion. This study is different from previous studies due to analysis of radar data from the newly constructed Xinyuan station. The results of this study provide an understanding of the macro- and microscale physical characteristics of clouds in the West Tianshan Mountains of Xinjiang in China in winter. Sect. 2 provides a brief introduction to the data and methodology used in this study. Sect. 3 presents the statistical results of the macroscopic characteristics and the microphysical properties of snowfall and non-snowfall clouds. Sect. 4 provides a discussion and a brief summary of the conclusions of the paper.

2 Data and methodology

2.1 Data

The observation period was 6 months in total (from January to February 2019, December 2019, and from December 2020 to February 2021), and all observation times were CST (China Standard Time, UTC + 8). The ground snowfall is measured by weighing the rain gauge at the Xinyuan weather station, and the unit is $\text{mm}\cdot\text{h}^{-1}$. An hourly precipitation amount $\geq 0.1 \text{ mm}\cdot\text{h}^{-1}$ was considered to be a precipitation occurrence. Then, the continuity of the snowfall clouds at the time of precipitation was judged according to the cloud radar map. If the clouds were continuous, one precipitation process was considered, and the number of hours from the beginning of the precipitation to the end was used to define the snowfall duration.

The manufacturer of the Ka-band millimeter-wave cloud radar is the Beijing Institute of Radio Measurement, and the model is HMB-KPS. The Ka radar works 24 h d^{-1} in a vertically pointing mode, as shown in Fig. 1. The parameters that were calculated from the cloud radar data include reflectivity, radial velocity, and the heights of the cloud top and base. To obtain the cloud top and base data, first, the cloud radar data were subjected to quality control to remove interfering echoes and noise. The heights of the cloud top and base were obtained according to the method of Wu et al. (2017). The effective signal observed by cloud radar was used as the cloud boundary, and each radial data point of cloud radar was divided into a continuous effective data segment. If the distance between two adjacent echo segments was less than a certain threshold (90 m), the two segments were merged into one segment, and if the length of the segment was less than the set threshold (120 m), the segment was deleted. The lower edge of the continuous valid data segment is

considered the cloud base, and the upper edge is considered the cloud top. Because the cloud touches the ground during precipitation, only the cloud top height was selected. The other main parameter indexes are shown in Table 1. When Chen (2018) used millimeter-wave cloud radar to make snow observations, he found that attenuation can be neglected when dry snow was detected below the order of $2 \text{ mm}\cdot\text{h}^{-1}$. Because the snowfall events selected in the paper are dry snow, the attenuation effect of snowfall is not considered in this paper. The cloud radar and the weighing rain gauge are both located at the Xinyuan weather station, with a distance of 10 m between the two instruments.

According to the radar meteorological equation, the reflectivity factor depends on many parameters, and the measurement of different parameters will have errors, which will affect the reflectivity factor. Therefore, the intensity of the radar reflectivity factor also needs to be calibrated before it can be used for research. Using the internal test signal, the amplitude of the input test signal is changed, the receiving channel, the signal processing method, and the output result of the signal processor are tested at different pulses, and the input and output characteristics of the receiving system are analyzed. The test result shows that the linearity of the receiving system is good.

2.2 Snowfall case selection

The currently used criteria for the magnitude of snowfall in Xinjiang are listed as follows: light snow, $0.1 \text{ mm} \leq \text{snowfall amount (R, hereinafter)} \leq 3.0 \text{ mm}$; moderate snow, $3.1 \text{ mm} \leq R \leq 6.0 \text{ mm}$; heavy snow, $6.1 \text{ mm} \leq R \leq 12.0 \text{ mm}$; snowstorm, $12.1 \text{ mm} \leq R \leq 24.0 \text{ mm}$; torrential snowstorm, $24.1 \text{ mm} \leq R \leq 48.0 \text{ mm}$; and severe snowstorm, $R \geq 48.1 \text{ mm}$ (Liu et al. 2021). In this study, the snowfall in the Xinyuan area between 2019 and 2020 was categorized according to these criteria. A total of 26 snowfall events

Table 1 Main performance indexes of the Ka-band millimeter-wave cloud radar system

No	Parameters	Index
1	Frequency	$35 \text{ GHz} \pm 500 \text{ MHz}$
2	Beam width	$\leq 0.4^\circ$
3	Transmit power	$\leq 500 \text{ W}$
4	Antenna gain	$\geq 52 \text{ dB}$
5	Antenna diameter	1.8 m
6	Height coverage	0.15–15 km
7	Temporal resolution	1 min
8	Range resolution	30 m
9	Polarization mode	Single-shot and single-take-up polarization
10	Emission wavelength	8.6 mm

were identified, including 15 light snow events, 7 moderate snow events, and 4 heavy snow events. Since the temporal resolution of the cloud radar was 1 min, the snowfall per min was taken as an observation sample. Thus, a total of 15,300 effective snowfall observation samples were obtained, including 4860, 6720, and 3720 samples of light, moderate and heavy snow, respectively. In addition, 30,060 observation samples of non-snowfall clouds were obtained. The magnitudes, periods, durations, and amounts of snowfall are summarized in Table 2. The average snowfall duration of light snow was 5.4 h, with a maximum duration of 13 h. The average snowfall amount of light snow was 1.13 mm. The average snowfall duration of moderate snow was 17 h, with a maximum duration of 25 h. The average snowfall amount of moderate snow was 3.98 mm. The average snowfall duration of heavy snow was 15.5 h, with a maximum duration of 27 h. The average snowfall amount of heavy snow was 7.75 mm. The average hourly snowfall amounts of light, moderate and heavy snow were $0.209 \text{ mm}\cdot\text{h}^{-1}$, $0.234 \text{ mm}\cdot\text{h}^{-1}$, and $0.5 \text{ mm}\cdot\text{h}^{-1}$, respectively (the average hourly snowfall amount = the total snowfall amount for the given snowfall magnitude / total snowfall duration).

2.3 Normalized contoured frequency by altitude diagram

Yuter and Houze (1995) employed a statistical technique based on the contoured frequency by altitude diagram (CFAD) to display the statistical distribution of storm properties for the first time. However, the CFAD method has the side effect of increasing the percentages at altitudes, where there are fewer data points. To overcome this weakness, many studies (Luo et al. 2009; Fu et al. 2003; Yuan et al. 2011; Guo et al. 2018) have suggested an improved statistical technique known as the normalized contoured frequency by the altitude diagram (NCFAD). The improvement is that the frequency for each box is normalized to the total number of points in all level boxes in the altitude phase space. Based on the total radar reflectivity, radial velocity, and particle water content at all height levels, the vertical structure of the cloud at the snowfall time was investigated using the NCFAD statistical method to calculate the proportions of radar reflectivity, radial velocity, and particle water content values at a certain height level within a certain numerical range in this study. The NCFAD is calculated as follows:

$$NCFAD = \frac{N_z(i,j)}{\sum_{i=1}^h \sum_{j=1}^n N_z(i,j)} \quad (1)$$

where $N_z(i,j)$ is a frequency distribution function that is defined as the occurrences of the j th reflectivity, radial velocity, and particle water content in the i th height layer. Because the layers below 150 m constitute the blind zone of

Table 2 Periods, durations, and amount of snowfall in snowfall events of different magnitudes

Magnitude	Time period	Duration (h)	Snowfall amount (mm)
Light	2019.01.29.06–2019.01.29.07	1	0.2
	2019.02.15.21–2019.02.16.11	14	2.1
	2019.11.25.19–2019.11.25.21	2	0.5
	2019.11.27.11–2019.11.27.12	1	0.3
	2019.12.20.10–2019.12.20.15	5	1.6
	2019.12.24.07–2019.12.24.14	7	0.6
	2020.12.05.01–2020.12.05.11	10	2.2
	2020.12.06.01–2020.12.06.04	3	1.1
	2020.12.08.01–2020.12.88.03	2	1.3
	2020.12.10.18–2020.12.10.21	3	0.8
	2020.12.21.14–2020.12.21.16	2	0.5
	2021.01.13.13–2021.01.13.22	9	1.8
	2021.01.24.10–2021.01.24.15	5	1.1
	2021.01.25.05–2021.01.25.09	4	0.7
	2021.02.25.11–2021.02.25.24	13	2.2
	Average	5.4	1.13
	Moderate	2019.02.10.17–2019.02.11.03	10
2019.02.12.11–2019.02.12.23		12	3.2
2019.02.21.10–2019.02.22.08		22	4.2
2019.11.07.19–2019.11.08.06		10	4.1
2019.12.22.06–2019.12.23.01		19	3.8
2020.12.27.03–2020.12.28.04		25	4.6
2021.01.14.03–2021.01.14.17		14	3.4
Average		17	3.98

Table 2 (continued)

Magnitude	Time period	Duration (h)	Snowfall amount (mm)
Heavy	2019.02.01.00– 2019.02.02.03	27	11.5
	2019.02.06.10– 2019.02.06.20	10	8.0
	2021.01.22.20– 2021.01.23.10	14	11.7
	2021.02.10.03– 2021.02.10.14	11	7.8
	Average	15.5	7.75

the millimeter-wave cloud radar, only data above 150 m were used in this study. In the NCFAD, the Y-axis constitutes the height index. For calculation and statistical convenience, we adjusted the vertical resolution from 30 to 150 m, and the total number of layers was 80. The X-axis of the NCFAD are reflectivity, radial velocity, and particle water content, with intervals of 1 dBZ, 0.25 m·s⁻¹, and 0.005 g·m⁻³, respectively. All cases for each cloud category were normalized in this paper.

2.4 Cloud radar parameters

Reflectivity is the total sum of the 6th power of the diameters of the particles within the unit volume, which is designated by Z (units, mm⁶·m⁻³). Because reflectivity can vary greatly, over several orders of magnitude, dBZ is used to represent the value of reflectivity:

$$dBZ = 10 \cdot \lg \frac{Z}{Z_0} \quad (Z_0 = 1mm^6 \cdot m^{-3}) \quad (2)$$

V represents the radial velocity of particles when the radar is oriented vertically: a positive value indicates upward velocity, and a negative value indicates the opposite.

2.5 Inversion of the water content of snow particles

The liquid water content in the clouds is a particularly important meteorological element, and its magnitude and spatial distribution serve as a crucial index for investigating the dynamics of clouds, as they reflect the degree of condensation and development in the clouds (Mason and Basil 1957). To date, there is a lack of methods for accurately measuring the magnitude of the liquid water content. However, the relative magnitude and spatial distribution of the liquid water content could be measured by radar, which requires assumptions about the drop spectrum in the cloud.

The water content of snow particles can also be calculated in a similar way. Marshall and Palmer (1948) proposed the Marshall–Palmer drop spectral distribution (M–P distribution). Based on the M–P distribution (Greene and Clark 1972), the liquid water content (M) and radar reflectivity (Z) can be represented as follows:

$$M = \frac{\rho\pi}{6} \int_0^x n(D)D^3 dD \quad (3)$$

$$Z = \int_0^x n(D)D^6 dD \quad (4)$$

where x represents the maximum drop diameter, D is the diameter, and ρ represents the water density. Under certain conditions, ice crystals collide with each other and merge to form snowflakes. During this aggregation growth, the temperature and the shape of the ice and snow crystals play primary roles. According to Gunn and Plamer (1958), the snowflake-scale relation approaches the M–P distribution at the time of precipitation, and the calculation is described as follows:

$$n(D_0) = n_0 \exp(-\Lambda D_0) \quad (5)$$

where $\Lambda = 25.5I^{-0.48}$, $n_0 = 3.8 \times 10^3 I^{-0.87}$, D_0 is the equivalent diameter of the water drop after snow melting (unit, mm), and I is the precipitation rate (unit, mm·h⁻¹), which is presented as the thickness of the obtained water after melting of the accumulated snow. Equations (3), (4) and (5) are combined, and the following simplified equation is obtained:

$$Z = AM^a \quad (6)$$

where the units of M are g·m⁻³, those of Z are mm⁶·m⁻³, and the coefficients A and a vary according to drop spectral patterns.

When the drops are snowflakes, $A = 3.8 \times 10^4$ and $a = 2.2$ (Zhang et al. 2001), and Eq. (6) can be described as follows:

$$M = 0.0083 \cdot 10^{0.0455 \cdot Z} \quad (7)$$

where the units of M and Z are g·m⁻³ and dBZ, respectively.

3 Results

3.1 Macrophysical characteristics of non-snowfall clouds

Figure 2 shows the diurnal variations in the base and top heights of the non-snowfall cloud observed in winter. The uppermost and lowermost points represent the maximum and minimum values, respectively. The transverse lines

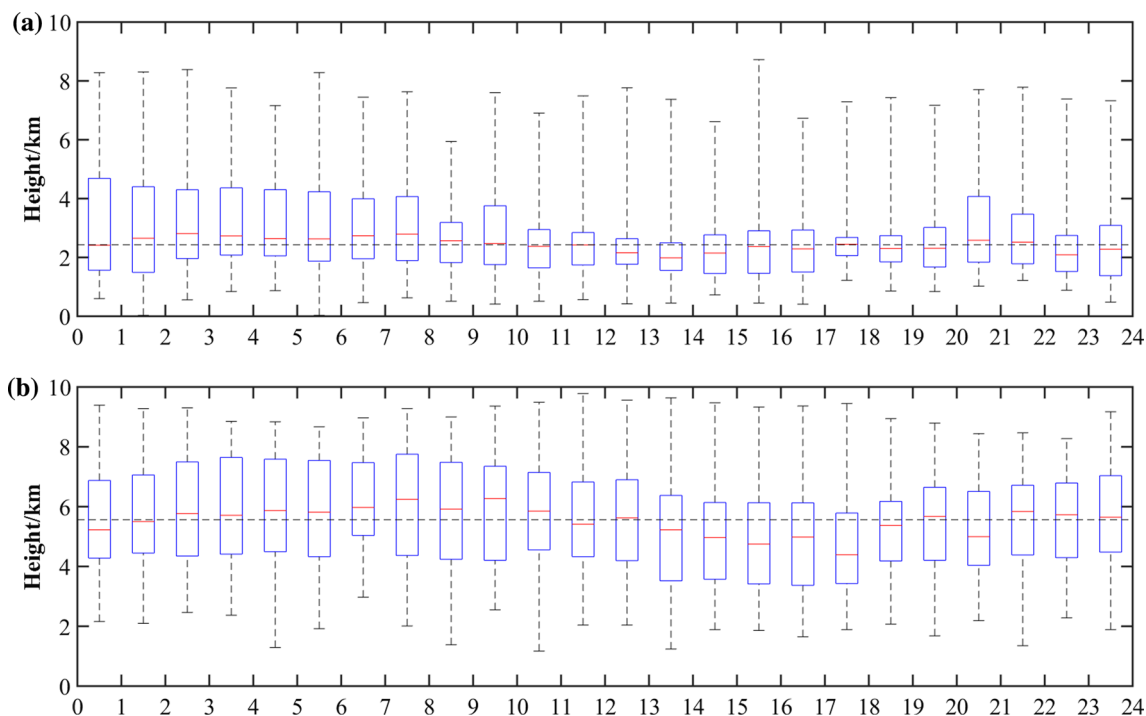


Fig. 2 Diurnal variations in the base (a) and top (b) heights of non-snowfall clouds in winter

of the box represent the 75% and 25% percentile values, respectively, and the middle line in the box represents the 50% percentile value. The black dotted lines represent the 50% percentile values of the base and top heights of all non-snowfall clouds. The local solar time of Xinyuan is 2.5 h later than that of CST. The median values of the base and top heights of the non-snowfall clouds were 2.43 km and 5.56 km, respectively. The base heights of the non-snowfall clouds displayed a low-height tendency during the daytime and a high-height tendency at night. The highest median value of the cloud base appeared during the period of 02:00–03:00 when the median value was 2.81 km. The median value of the base height of the cloud during 10:00–17:00 was lower than that of all clouds. The lowest median value, which was 1.98 km, appeared at 13:00–14:00 (Fig. 2a). The top heights of non-snowfall clouds displayed a low-height tendency during the daytime and a high-height tendency at night. The highest median value of the cloud top occurred during 09:00–10:00 (approximately 6.26 km) and the lowest median value occurred during 17:00–18:00 (4.39 km) (Fig. 2b). Higher daytime temperatures favor increased atmospheric instability. In addition, the trumpet-shaped topography on the west side of the observation point (Fig. 1) has an important influence on airflow through the Tianshan mountains. Mountain valley wind circulation (Zeng et al. 2020b), formed by a westerly wind blowing from the valley to the mountains during the daytime and an easterly wind blowing from the mountains to the valley

during the nighttime, may also play an important role. Under the influence of westerly winds during the daytime, the low-level airflow has climbing and ascending motion, and the heating effect of solar radiation increases the instability of the low-level atmosphere, thereby making the exchange of matter and energy in the boundary layer more active. Under such dynamic and thermal conditions, daytime clouds tend to form at lower altitudes. In contrast, cold air from the top of the mountain moves down and westward at night, and the sinking motion combined with the lower temperatures stabilizes the lower atmosphere, which is not conducive to the formation of lower atmosphere clouds. At the same time, some higher clouds near the summit moved over Xinyuan under the influence of easterly winds. The above physical processes cause cloud base heights and cloud top heights to be higher at night than during the day.

Figure 3 shows the distributions of the base and top heights of non-snowfall clouds in winter. Both the cloud base and cloud top values exhibit single-peak distributions. The cloud base heights (CBH) of the clouds were primarily distributed within the range of 1~4 km, and the probability of the appearance of the cloud base at any height level within this range was greater than 10%. The highest occurrence frequency of the cloud base was observed at the height level of 2~3 km, with a value of 35.4%, whereas the lowest frequency was observed at the height level of 8~9 km, with a value of 0.12% (Fig. 3a). The cloud top heights (CTH) were primarily distributed within the height

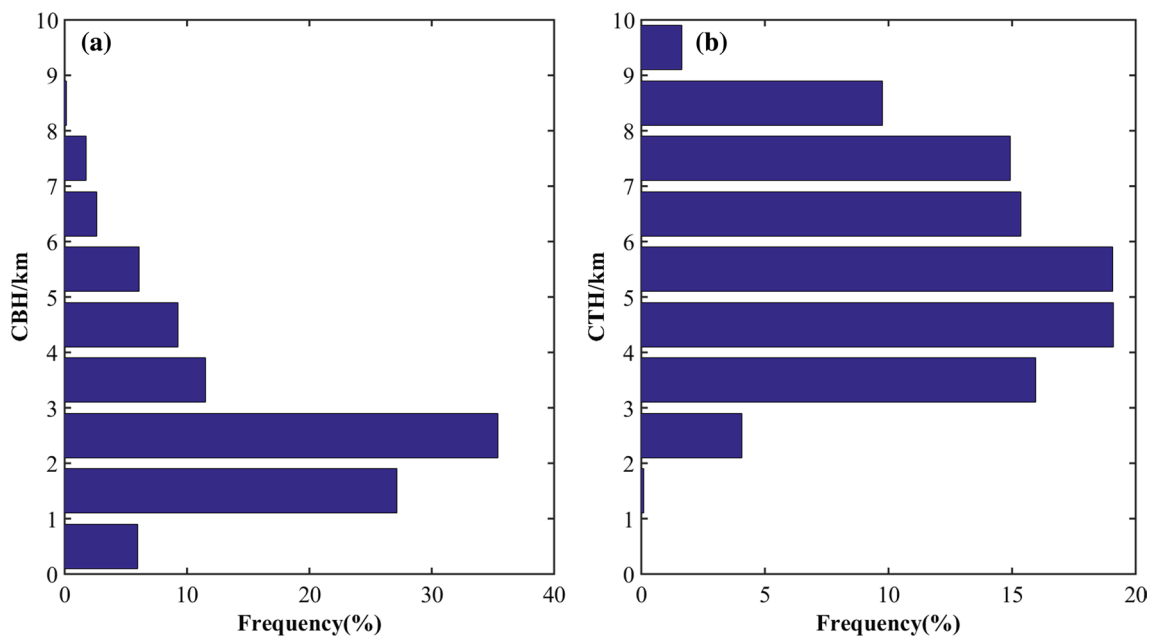


Fig. 3 Distributions of the base (a) and top (b) heights of non-snowfall clouds in winter

range of 3~8 km, and the probability of the appearance of the cloud top at any height level within this range was greater than 10%. The highest occurrence frequency of the cloud top was observed at the height level of 4~5 km, with a value of 19.1%, whereas the lowest frequency was observed at the height level of 1~2 km, with a value of approximately 0.11% (Fig. 3b).

3.2 Macrophysical characteristics of snowfall clouds

Figure 4 shows the diurnal variations in the top and distributions of the snowfall clouds observed in winter. The median value of the top height of the snowfall cloud is 5.1 km. The median top altitudes of the snowfall clouds in different periods range from 3.9 km to 6.9 km. The highest median value occurs during 23:00–24:00, and the lowest median value occurs during 05:00–06:00 (Fig. 4a). The cloud top values exhibit bimodal distributions. The cloud tops are primarily distributed within the altitude range of 3~6 km and 7~9 km, and the probability of the appearance of the cloud top at any height level within this range is greater than 10%. The highest occurrence frequency of the cloud top was observed at the height level of 3~4 km, with a value of 24.6%, whereas the lowest frequency was observed at the height level of 1~2 km, with a value of approximately 0.55% (Fig. 4b). The cloud top heights of snowfall clouds are lower than those of non-snowfall clouds, which may be due to the lower atmospheric instability due to the reflection of solar radiation by clouds during snowfall due to the high cloud cover.

3.3 Microphysical characteristics of non-snowfall clouds

Because the observations in this study were performed in winter when the temperature was low, we inverted the M values of the non-snowfall clouds in accordance with Eq. (7). Figure 5 shows the NCFADs of the Z, V, and M of the non-snowfall clouds in winter. Under non-snowfall conditions, clutters existed in the bottom air within a certain height range. Therefore, we extracted only the radar parameters above 0.48 km for investigation. Most of the non-snowfall clouds did not extend to the ground, and the maximum cloud top extended above 10 km. In addition, the maximum Z exceeded 20 dBZ (with most of the Z values being less than 20 dBZ) (Fig. 5a). The non-snowfall clouds were mainly distributed in 2~8 km, and the Z values were within the range of -22~15 dBZ. The maximum frequency center appeared at 2.5~6.5 km, with Z values within the range of -14~-14 dBZ (Fig. 5a). The V values of the non-snowfall clouds were mainly within -1.1~-0.4 m·s⁻¹, and the clouds were mainly located at 2.0~7.5 km (Fig. 2b). The M values were primarily less than 0.018 g·m⁻³ within the height range of 1.2~8.7 km, with a maximum M value of 0.02 g·m⁻³ (Fig. 5c).

3.4 Microphysical characteristics of snowfall clouds

Figures 6 shows the NCFADs of the Z, V and M of snowfall clouds in winter during the observations. As shown in Fig. 6a, the proportion of snowfall clouds above 4 km

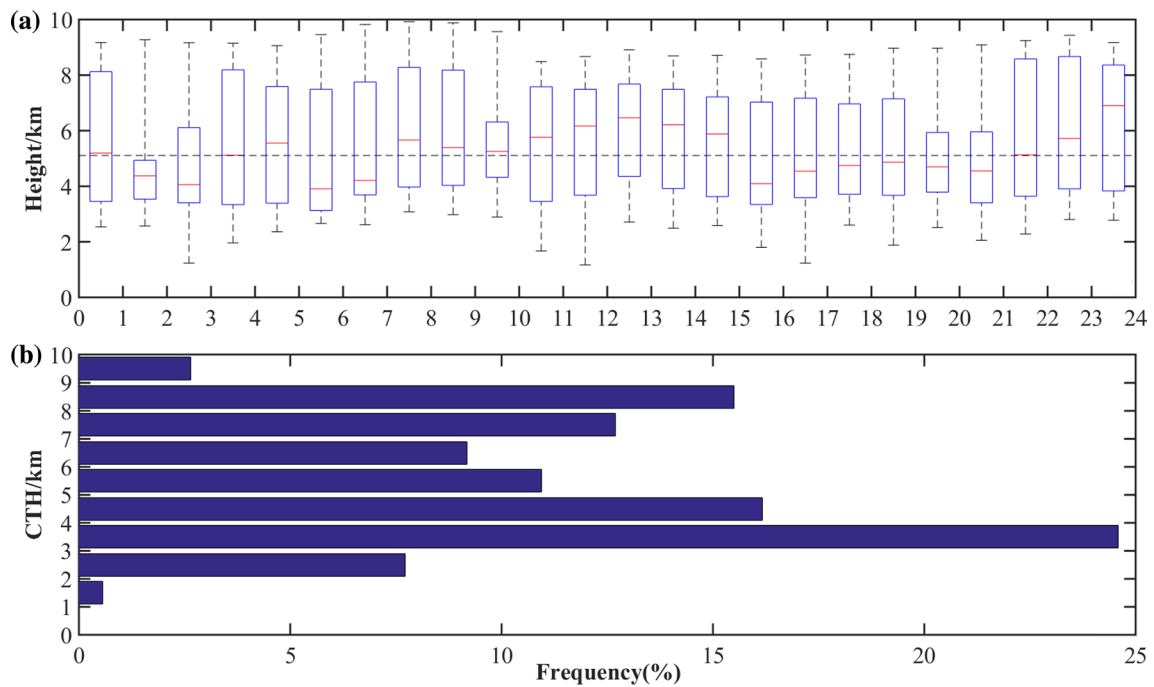


Fig. 4 Diurnal variations in the top height (a) and distributions of the top height (b) of snowfall clouds

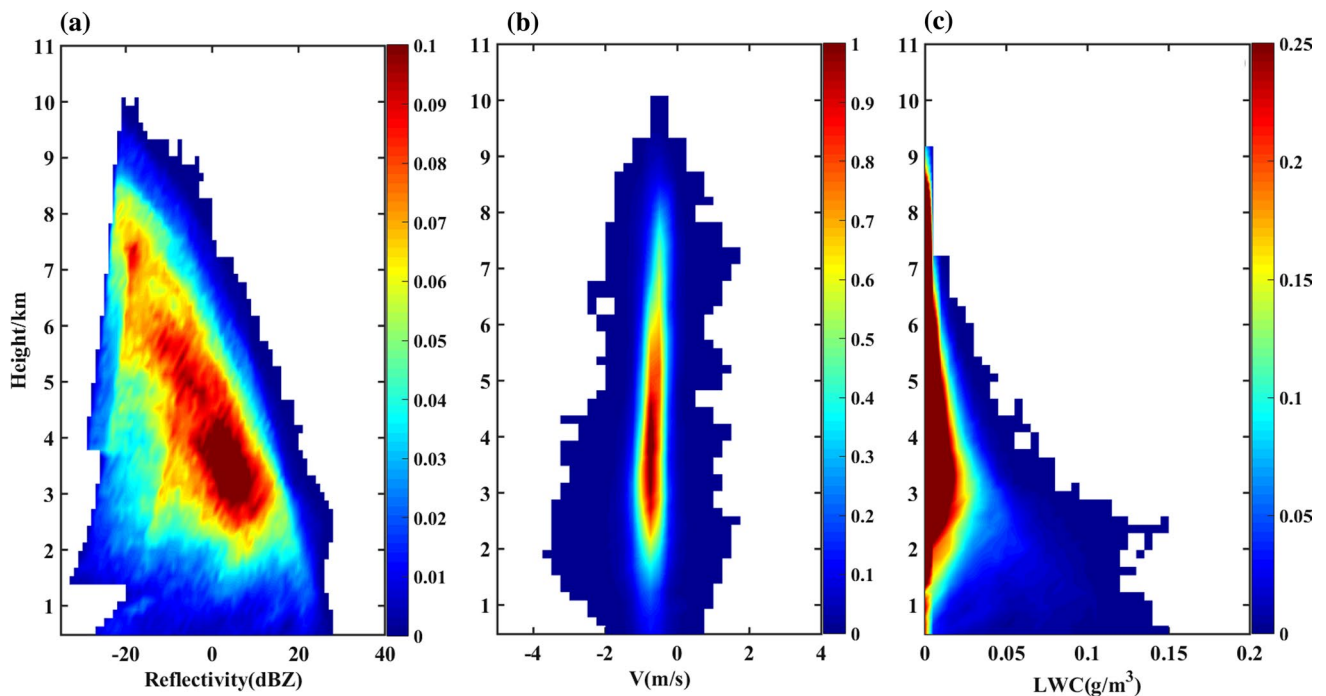


Fig. 5 Normalized contoured frequency by altitude diagrams of the cloud radar parameters of the non-snowfall clouds in winter (unit, %). **a** Z. **b** V. **c** M

relative to the total number of clouds was small, and the Z values of clouds above 7.5 km were basically below 0 dBZ. The snowfall clouds were primarily distributed from 0.15~2.50 km, the Z values of the clouds were 10~23 dBZ,

and the maximum Z value reached 37 dBZ (Fig. 6a). The V values of snowfall clouds were between $-5 \text{ m}\cdot\text{s}^{-1}$ and $4 \text{ m}\cdot\text{s}^{-1}$, mainly distributed in the range from 0.15 km to 3.50 km and concentrated in the range of $-1.2 \sim -0.4 \text{ m}\cdot\text{s}^{-1}$

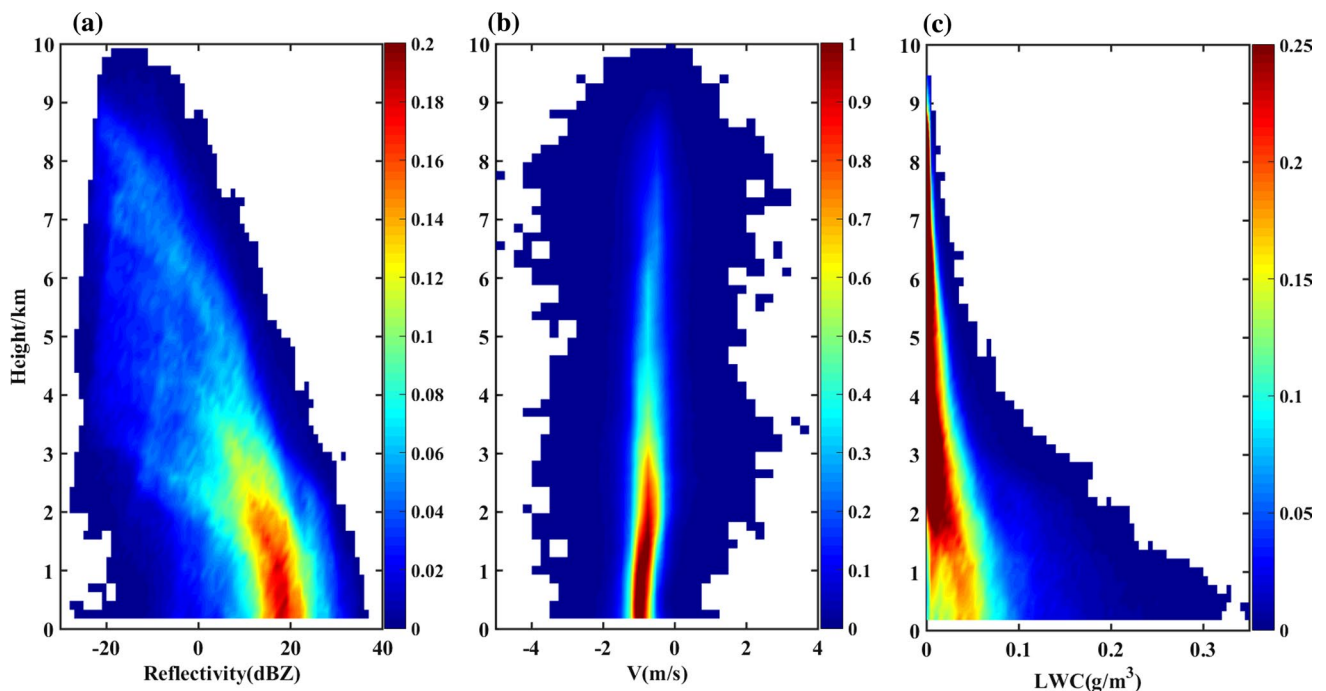


Fig. 6 Normalized contoured frequency by altitude diagrams of radar parameters of snowfall clouds (unit: %). **a** Z. **b** V. **c** M

(Fig. 6b). The maximum M of snowfall clouds was $0.35 \text{ g}\cdot\text{m}^{-3}$, mainly distributed from 1.9 to 8.9 km and concentrated below $0.03 \text{ g}\cdot\text{m}^{-3}$ (Fig. 6c). Compared with the non-snowfall clouds, the snowfall cloud in winter were located at lower heights but had larger Z and M values, and the non-snowfall clouds generally did not reach the ground.

3.5 Microscale physical characteristics of clouds with different snowfall magnitudes

Figure 7 shows the NCFADs of the Z values of light snow, moderate snow, and heavy snowfall clouds. The snowfall clouds associated with light snow occupied a small proportion of the total number of clouds above 7 km, and the Z value above 7 km was generally less than 0 dBZ. The snowfall clouds associated with light snow were primarily distributed between 0.15 km and 3.50 km, and the Z values were primarily between 5 and 23 dBZ, with a maximum value of 31 dBZ (Fig. 7a). The snowfall clouds associated with moderate snow occupied a small proportion of the total number of clouds above 7 km, and the Z values above 7 km were generally less than 0 dBZ. These snowfall clouds were primarily distributed between 0.15 km and 2.50 km. The Z values were mostly between 5 and 24 dBZ, with a maximum of 32 dBZ (Fig. 7b). The snowfall clouds associated with heavy snow occupied a small proportion of the total number of clouds above 8 km, and the Z values above 8 km were generally less than 0 dBZ. These snowfall clouds were primarily distributed between 0.15 km and 3.50 km. The Z

values were primarily between 5 and 30 dBZ, and the maximum Z values reached 36 dBZ (Fig. 7c). As shown in Fig. 7, the NCFADs of light snow, moderate snow and heavy snow were similar. However, below 2 km, the Z values of heavy snow were noticeably higher than those of light snow and moderate snow, which could reach 17~30 dBZ. This result occurred, because the average hourly snowfall amount of heavy snow was much larger than that of any other snowfall type.

Figure 8 shows the NCFADs of the V values of light snow, moderate snow, and heavy snowfall clouds. As shown in Fig. 8, downward motions under all magnitudes of snowfall were gathered primarily below 6 km. The V values of the snowfall clouds were mainly distributed at $-1.4 \sim -0.3 \text{ m}\cdot\text{s}^{-1}$. The variation range of the V values of moderate snow clouds was the smallest. Snowfall events of different magnitudes did not show noticeable differences in the range of the radial velocity.

Figure 9 shows the NCFADs of the M values of light snow, moderate snow, and heavy snowfall clouds. Light snow M was mainly located at 0.15~8.50 km, and most of the M values in these layers were less than $0.06 \text{ g}\cdot\text{m}^{-3}$, with the highest value of $0.2 \text{ g}\cdot\text{m}^{-3}$ (Fig. 9a). The moderate snow M was primarily distributed from 0.15~8.50 km, and most of the M values in these layers were less than $0.06 \text{ g}\cdot\text{m}^{-3}$, with the highest value of $0.23 \text{ g}\cdot\text{m}^{-3}$ (Fig. 9b). The heavy snow M was mainly distributed in 1.0~9.0 km, and most of the M values in these layers were less than $0.06 \text{ g}\cdot\text{m}^{-3}$, with the highest value of $0.35 \text{ g}\cdot\text{m}^{-3}$ (Fig. 9c). The proportion of

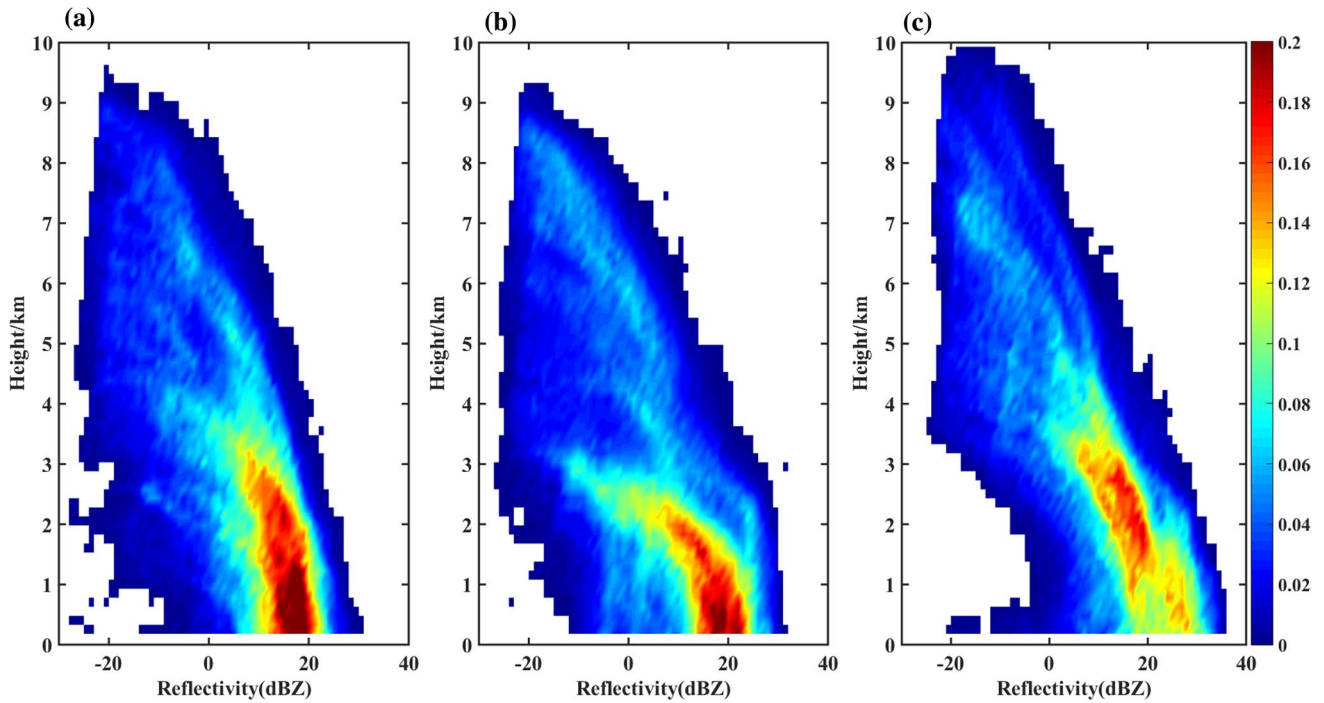


Fig. 7 Normalized contoured frequency by altitude diagrams of snowfall cloud Z (unit: %). a Light snow. b Moderate snow. c Heavy snow

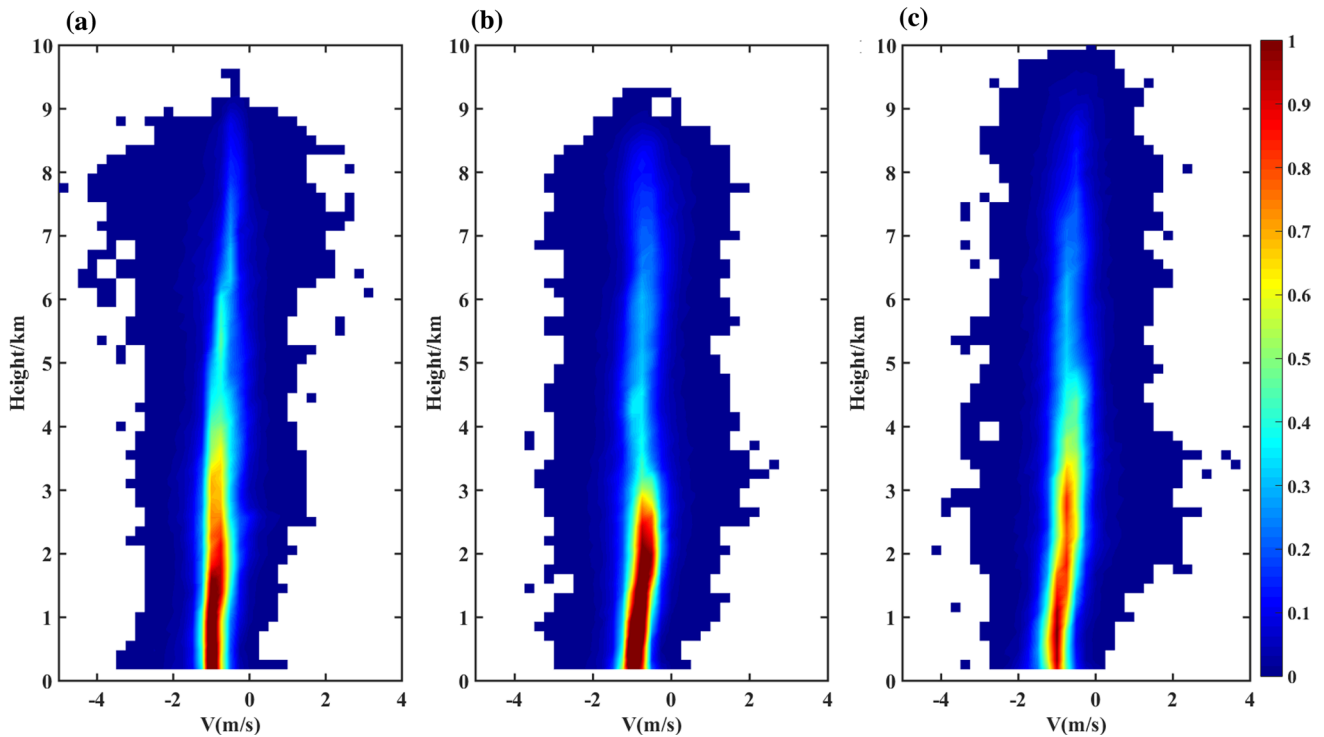


Fig. 8 Normalized contoured frequency by altitude diagrams of snowfall cloud V (unit: %). a Light snow. b Moderate snow. c Heavy snow

clouds with an M value $> 0.1 \text{ g}\cdot\text{m}^{-3}$ below 2 km under heavy snow was markedly higher than that in any other snow type,

and the variation range of M increased with the magnitude of snowfall. These findings indicate that the moisture content

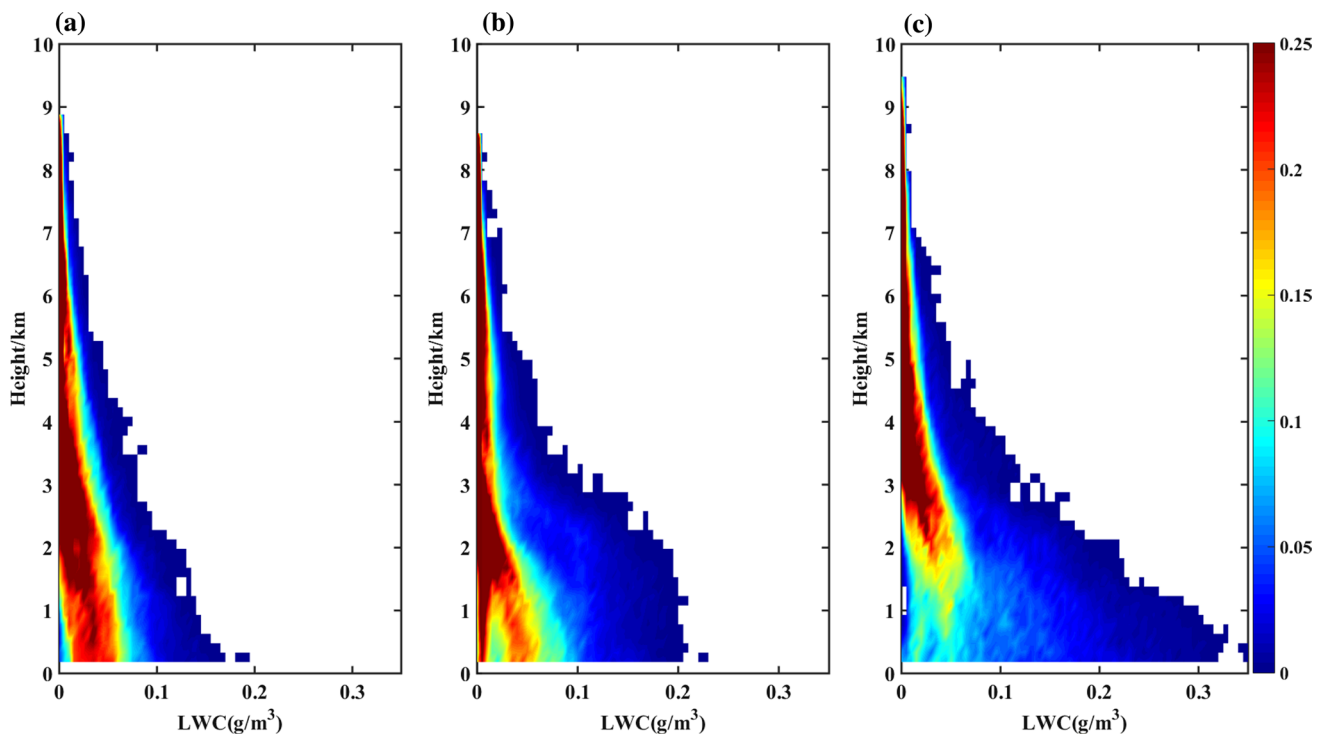


Fig. 9 Normalized contoured frequency by altitude diagrams of snowfall cloud M above (unit: %). **a** Light snow. **b** Moderate snow. **c** Heavy snow

in light snow was low, that a small amount of water vapor was available for the snow process, and that light snow had the shortest average duration. The moisture content of heavy snow was the highest among the three snow types; thus, sufficient water vapor was available for the heavy snow process, and heavy snow had the longest average duration.

4 Conclusions and discussion

In this study, we analyzed the structural characteristics of snowfall clouds and non-snowfall clouds in the West Tianshan Mountains of China in winter from January to February 2019, December 2019, and from December 2020 to February 2021 based on cloud radar data. The main conclusions are as follows:

- (1) Snowfall clouds were primarily distributed within the height range of 0.15 ~ 2.50 km and had reflectivity (Z) mainly between 10 and 33 dBZ. Non-snowfall clouds were primarily distributed within the height range of 2 ~ 8 km, and the Z values were within the range of - 22 ~ 15 dBZ. Compared with non-snowfall clouds, snowfall clouds have higher particle water content (M), but the V values were similar.
- (2) Light and moderate snowfall clouds were primarily distributed between 0.15 km and 3.50 km, and the Z

- values were primarily between 5 and 24 dBZ. Heavy snowfall clouds were characterized by a Z of 5 ~ 30 dBZ below 3.5 km. Although the NCFADs of the Z values were similar among the three snow types, the Z values below 2 km during heavy snow were noticeably higher than those during light and moderate snow. The underlying reason for this occurrence was that average hourly snowfall of heavy snow was markedly greater than that of light and moderate snow.
- (3) The proportion of snowfall clouds with $M > 0.1 \text{ g}\cdot\text{m}^{-3}$ below 2 km during heavy snowfall was noticeably higher than those during light snow and moderate snow. The M during light snow was the lowest among the three snow types, indicating that a small amount of water vapor was available. Therefore, the average duration of light snow was the shortest. In contrast, during heavy snow, M was high, indicating that sufficient water vapor was available. For this reason, the average duration of heavy snow was the longest.
 - (4) The height of the non-snowfall cloud top and base during the day was lower than at night. The snowfall cloud top did not show noticeable diurnal variations. The cloud top and base of the non-snowfall clouds both showed a single-peak distribution. The cloud top values of snowfall exhibited bimodal distributions.

The characteristics of clouds and precipitation are important for understanding the formation process for clouds and precipitation (Ackerman and Stokes 2003; Harrison et al. 1990; Schiffer and Rossow 1983; Zhang et al. 2019a). In the past, many researchers have studied the macro- and microphysical properties of rainfall clouds and non-rainfall clouds, and the conclusions of these studies help to understand clouds and precipitation. However, previous studies have mainly focused on areas with abundant rainfall (Zhang et al. 2019b; Luo et al. 2009; Yi 2013; Liu et al. 2015; Ma et al. 2018; Cui et al. 2020; Yue et al. 2020; Wang et al. 2018; Huo et al. 2020a, b; Wu et al. 2020) and there have been few studies on arid areas instead. In recent years, an increasing number of studies on precipitation and non-precipitation cloud macro- and microphysical properties have been carried out in the arid regions of China, especially in the Qinghai–Tibet Plateau (Yi 2019; Liu et al. 2021; Ma et al. 2018; Qiu et al. 2018; Zhao et al. 2016, 2017), but less research has been carried out in Xinjiang. Therefore, the findings of this paper deepen the understanding of winter clouds in the West Tianshan Mountains of China and provide useful data for further investigation of the structural characteristics of winter clouds in this region.

Many scholars have conducted similar studies on snowfall clouds in monsoon regions, and the results are somewhat similar and different from those in the West Tianshan Mountains of China. For example, the precipitation cloud Z in winter in the West Tianshan Mountains is generally larger than that in Beijing (Zhang et al. 2019b). The range of V during snowfall in Shou County (Cui et al. 2020) is similar to that in the West Tianshan Mountains of China, indicating that the falling velocities of snow particles in the two regions are similar. The concentration area of snowfall cloud Z in winter is lower than that in East Asia (Yin et al. 2013). This phenomenon might be caused by the collision of snowfall clouds that play a large role in the low air, increasing snowfall cloud particles in western China.

Different from the existing classification of cloud macro- and microphysical characteristics analysis, according to the snowfall classification criteria, the winter snowfall in the West Tianshan Mountains of China was divided into light snow, moderate snow, and heavy snow. The similarities and differences in the microphysical characteristics of the Z, V, and M of these three types of snowfall clouds were analyzed. Meanwhile, the structural characteristics of snowfall clouds and non-snowfall clouds in winter were also analyzed.

However, the macro- and microphysical characteristics of winter clouds were based only on the parameters Z, V, and M. Further studies in this area involving more microscale physical parameters, such as particle radius and particle content, should be conducted in the future.

Acknowledgements This research was funded by the first National Natural Science Foundation of China program number (U2003106), National Key Research and Development Program of China (2018YFC1507102), Central Asian Atmospheric Science Research Fund (CASS201715) and Xinjiang Uygur Autonomous Region Introduces High-level Talents Tianchi Project (2019).

Author contributions Methodology, J.Z.; formal analysis, J.Z, H.L and Y.Z; data curation, L.Y; writing—original draft preparation, J.Z; writing—review and editing, H.L, L.Y and J.L; funding acquisition, L.Y and J.L. All authors have read and agreed to the published version of the manuscript.

Data availability The data sets generated during and analyzed during the current study are available from the corresponding author on reasonable request.

Declarations

Competing interest The authors declare that they have no known competing financial interests or personal relationships that could have appeared to influence the work reported in this paper.

Open Access This article is licensed under a Creative Commons Attribution 4.0 International License, which permits use, sharing, adaptation, distribution and reproduction in any medium or format, as long as you give appropriate credit to the original author(s) and the source, provide a link to the Creative Commons licence, and indicate if changes were made. The images or other third party material in this article are included in the article's Creative Commons licence, unless indicated otherwise in a credit line to the material. If material is not included in the article's Creative Commons licence and your intended use is not permitted by statutory regulation or exceeds the permitted use, you will need to obtain permission directly from the copyright holder. To view a copy of this licence, visit <http://creativecommons.org/licenses/by/4.0/>.

References

- Ackerman TP, Stokes GM (2003) The atmospheric radiation measurement program. *Phys Today* 56(1):38–44
- Chen S, Kerns BW, Guy N et al (2016) Aircraft Observations of dry air, the ITCZ, convective cloud systems, and cold pools in MJO during DYNAMO. *Bull Am Meteorol Soc* 97:405–423
- Chengwu L, Dawei An, Junlan Z et al (2021) Variation Characteristics of Different Levels of Snowfall in Winter over Northern Xinjiang from 1961 to 2019. *Desert and Oasis Meteorology* 15(4):115–122 ((In Chinese))
- Clement AC, Burgman R, Norris JR (2009) Observational and model evidence for positive low-level cloud feedback. *Science* 325(5939):460–464
- Cui Y, Ruan Z, Wei M et al (2020) Vertical Structure and Dynamical Properties during Snow Events in Middle Latitudes of China from Observations by the C-band Vertically Pointing Radar. *J Meteorol Soc Japan* 98(3):527–550
- Fu Y, Lin Y, Liu G et al (2003) Seasonal characteristics of precipitation in 1998 over East Asia as derived from TRMM PR. *Adv Atmos Sci* 20(4):511–529
- Greene DR, Clark RA (1972) Vertically integrated liquid water—a new analysis tool. *Mon Wea Rev* 100(7):548
- Gunn KLS, Plamer WM (1958) The distribution with size of aggregate snowflakes. *J Atmos Sci* 15(5):452–461

- Guo JP, Liu H, Li ZQ et al (2018) Aerosol-induced changes in the vertical structure of precipitation: a perspective of TRMM precipitation radar. *Atmos Chem Phys* 18(18):13329–13343
- Haifei Li, Man Y, Feiyue Y et al (2017) Analysis on Macroscopic Characteristics of Winter Cloud in Huainan Area of Anhui Based on Ground-based Cloud Radar Data. *J Arid Meteorol* 35(6):1011–1014 ((in Chinese))
- Harrison EF, Minnis P, Barkstrom BR et al (1990) Seasonal variation of cloud radiative forcing derived from the Earth Radiation Budget Experiment. *J Geophys Res Atmos* 95(D11):18687–18703
- Huo J, Li J, Duan M et al (2020a) Measurement of cloud top height: comparison of MODIS and ground-based millimeter radar. *Remote Sens* 12(10):1616
- Huo J, Tian Y, Wu X et al (2020b) Properties of ice cloud over Beijing from surface Ka-band radar observations during 2014–2017. *Atmos Chem Phys* 20(22):14377–14392
- Kollias P, Jasmine LE et al (2011) Cloud radar Doppler spectra in drizzling stratiform clouds: 1. Forward modeling and remote sensing applications. *J Geophys Res*, 116
- Li H, Dmitri M, Annakaisa VL (2017) How Does Riming Affect Dual-Polarization Radar Observations and Snowflake Shape? *Journal of Geophysical Research Atmospheres* 123:6070–6081
- Li PJ (1998) The temporal and spatial distribution of snow disaster over the Tibetan Plateau. Beijing: China Meteorological Press 15–18pp (In Chinese)
- Liu LP, Zheng JF, Ruan Z et al (2021) Comprehensive radar observations of clouds and precipitation over the Tibetan Plateau and preliminary analysis of cloud properties. *Journal of Meteorological Research* 29(4):546–561
- Luo Y, Zhang R, Wang H (2009) Comparing Occurrences and Vertical Structures of Hydrometeors between Eastern China and the Indian Monsoon Region Using CloudSat/CALIPSO Data. *J Climate* 22(4):1052–1064
- Luo YL, Zhang RH, Qian WM et al (2011) Intercomparison of deep convection over the Tibetan Plateau-Asian monsoon region and subtropical North America in boreal summer using Cloud-Sat/CALIPSO data. *J Climate* 24(8):2164–2177
- Ma RY, Luo YL, Wang H (2018) Classification and diurnal variations of precipitation echoes observed by a C-band vertically-pointing radar in central tibetan plateau during TIPX-III 2014-IOP. *J Meteorol Res* 32(6):985–1001
- Marshall JS, Palmer WMK (1948) The distribution of raindrops with size. *J Meteorol* 5(4):165–166
- Mason BJ (1957) *The Physics of Clouds*. Oxford University Press, London, p 481
- Parish TR, Leon D (2013) Measurement of cloud perturbation pressures using an instrumented aircraft. *Atmos Ocean Tech* 30(2):215–229
- Qie XS, Wu XK, Yuan T et al (2014) Comprehensive pattern of deep convective systems over the Tibetan Plateau-South Asian monsoon region based on TRMM data. *J Climate* 27(17):6612–6626
- Qiu Y, Lu C, Shi L (2018) Tibetan plateau cloud structure and cloud water content derived from millimeter cloud radar observations in summer. *Pure Appl Geophys* 176(D8):1785–1796
- Reddy NN, Ratnam MV, Basha G et al (2018) Cloud vertical structure over a tropical station obtained using long-term high-resolution radiosonde measurements. *Atmos Chem Phys* 18:11709–11727
- Schiffer R A, Rossow W B (1983) *The International Satellite Cloud Climatology Project (ISCCP) - The first project of the World Climate Research Programme*. *Bull.amer.meteor.soc* 64(7):779–784
- Wang L, Liu L, Yu J et al (2017) Microphysics and dynamic characteristic analysis of freezing rain and snow observed by Millimeter-Wave Radar. *Meteorol Month* 43(12):1473–1486 ((in Chinese))
- Wang Z, Wang Z, Cao X et al (2018) Comparison of cloud top heights derived from FY-2 meteorological satellites with heights derived from ground-based millimeter wavelength cloud radar. *Atmos Res* 199:113–127
- Wu P, Dong X, Xi B et al (2020) Profiles of MBL Cloud and Drizzle Microphysical Properties Retrieved From Ground-based Observations and Validated by Aircraft In Situ Measurements Over the Azores. *J Geophys Res Atmos* 125(9):e2019JD032205
- WuLiu CL, Zhai XC (2017) The comparison of cloud base observations with Ka-band solid-state transmitter-based millimeter wave cloud radar and ceilometer in summer over Tibetan Plateau. *Chin J Atmos Sci* 41(4):659–672 ((in Chinese))
- Xu WX (2013) Precipitation and convective characteristics of summer deep convection over East Asia observed by TRMM. *Mon Wea Rev* 141(5):1577–1592
- Yi M (2019) Differences in Cloud Vertical Structures between the Tibetan Plateau and Eastern China Plains during Rainy Season as Measured by CloudSat/CALIPSO. *Adv Meteorol* 6:1–11
- Yin JF, Wang DH, Zha GQ et al (2013) Observational Characteristics of Cloud Vertical Profiles over the Continent of East Asia from the CloudSat Data. *Acta Meteor Sin* 27(1):26–39
- Yuan J, Houze RA, Heymsfield AJ (2011) Vertical structures of anvil clouds of tropical mesoscale convective systems observed by CloudSat. *J Atmos Sci* 68(8):1653–1674
- Yue Q, Jiang JH, Heymsfield A et al (2020) Combining In Situ and Satellite Observations to Understand the Vertical Structure of Tropical Anvil Cloud Microphysical Properties During the TC4 Experiment. *Earth Space Sci* 7(4):e2020EA001147
- Yuter SE, Houze RA (1995) Three-dimensional kinematic and microphysical evolution of Florida cumulonimbus. Part II: Frequency distributions of vertical velocity, reflectivity, and differential reflectivity. *Mon. Wea. Rev* 123(7):1921–1940
- Zeng Y, Yang L, Tong Z et al (2020a) 2020a) Application of Multiple Detection Data in the Analysis of Snowstorm Processes in Xinjiang during the Central Asia Extreme Precipitation Observation Test (CAEPOT). *Advances in Meteorology* 3:1–13
- Zeng Y, Yang LM, Zhang ZY et al (2020b) Characteristics of Clouds and Raindrop Size Distribution in Xinjiang, Using Cloud Radar Datasets and a Disdrometer. *Atmosphere* 11:1382
- Zhang PC, Du BY, Dai TP (2001) *Radar meteorology*. China Meteorological Press, Beijing, China ((In Chinese))
- Zhang A, Hu J, Chen S et al (2019a) Statistical Characteristics of Raindrop Size Distribution in the Monsoon Season Observed in Southern China. *Remote Sensing* 11(4):432
- Zhang Y, Zhou Q, Lv S et al (2019b) Elucidating cloud vertical structures based on three-year Ka-band cloud radar observations from Beijing, China. *Atmospheric Research* 222(JUL):88–99
- Zhao C, Liu L, Wang Q et al (2016) Toward Understanding the Properties of High Ice Clouds at Naqu Site over the Tibetan Plateau Using Ground-based Active Remote Sensing Measurements Obtained during a Short Period in July 2014. *J Appl Meteorol Climatol* 55(11):2493–2507
- Zhao C, Liu L, Wang Q et al (2017) MMCR-based characteristic properties of non-precipitating cloud liquid droplets at Naqu site over Tibetan Plateau in July 2014. *Atmos Res* 190:68–76
- Zhou C, Zelinka MD, Klein SA (2016) Impact of decadal cloud variations on the Earth's energy budget. *Nat Geosci* 9(12):871–874